Nodule

1

Solitary Pulmonary Nodule (SPN), Solid

Definition

Solitary pulmonary nodules (SPNs) are defined as focal, round, or oval areas of increased opacity in the lung with diameters of ≤3 cm [1] (Fig. 1.1). The lesion is not associated with pneumonia, atelectasis, or lymphadenopathy.

Particularly when the nodule is less than 10 mm in diameter, it may be called small nodule (Fig. 1.2). With its diameter less than 3 mm, it may be called micronodule [2].

Diseases Causing the Pattern

The most common cause is malignant tumor including *lung cancer* (Fig. 1.3), *carcinoid* (Fig. 1.4), *bronchus-associated lymphoid tissue* (*BALT*) *lymphoma* (Fig. 1.5), and a solitary metastasis to the lung. Benign tumors are *granuloma* (Fig. 1.6), *hamartoma* (Fig. 1.7), *sclerosing hemangiomas* (Fig. 1.8), *inflammatory myofibroblastic tumor* (*IMT*, *inflammatory pseudotumor*) (Fig. 1.9), rheumatoid nodule (Fig. 1.2), parasitic infection (*Paragonimus westermani*), and *nodule in antineutrophil cytoplasmic antibody* (*ANCA*)-*associated granulomatous vasculitis* (*former Wegener's granulomatosis*) (Fig. 1.10) (Table 1.1).

Fig. 1.1 A lung nodule representing lung adenocarcinoma with acinar- and papillary-predominant subtypes in a 52-year-old woman. Thin-section (2.5-mm section thickness) CT scan obtained at level of tracheal carina shows a 22-mm-sized nodule with lobulated and spiculated margin in the left upper lobe

Distribution

Likelihood ratio for malignancy in upper and middle lobe nodule is 1.22 as compared with 0.66 in lower lobe nodule [3].

Clinical Considerations

The hierarchy of radiologic and clinical likelihood ratios for malignancy includes, in decreasing rank, a cavity of 16 mm in thickness, irregular or speculated margin on CT scans, patient complaints of hemoptysis, a patient history of malignancy, patient age >70 years, nodule size of 21–30 mm in diameter, nodule growth rate of 7–464 days, an ill-defined nodule on chest radiographs, a currently smoking patient, and nodules with indeterminate calcification on CT scans [3].

K.S. Lee et al., *Radiology Illustrated: Chest Radiology*, Radiology Illustrated,
DOI 10.1007/978-3-642-37096-0_1, © Springer-Verlag Berlin Heidelberg 2014

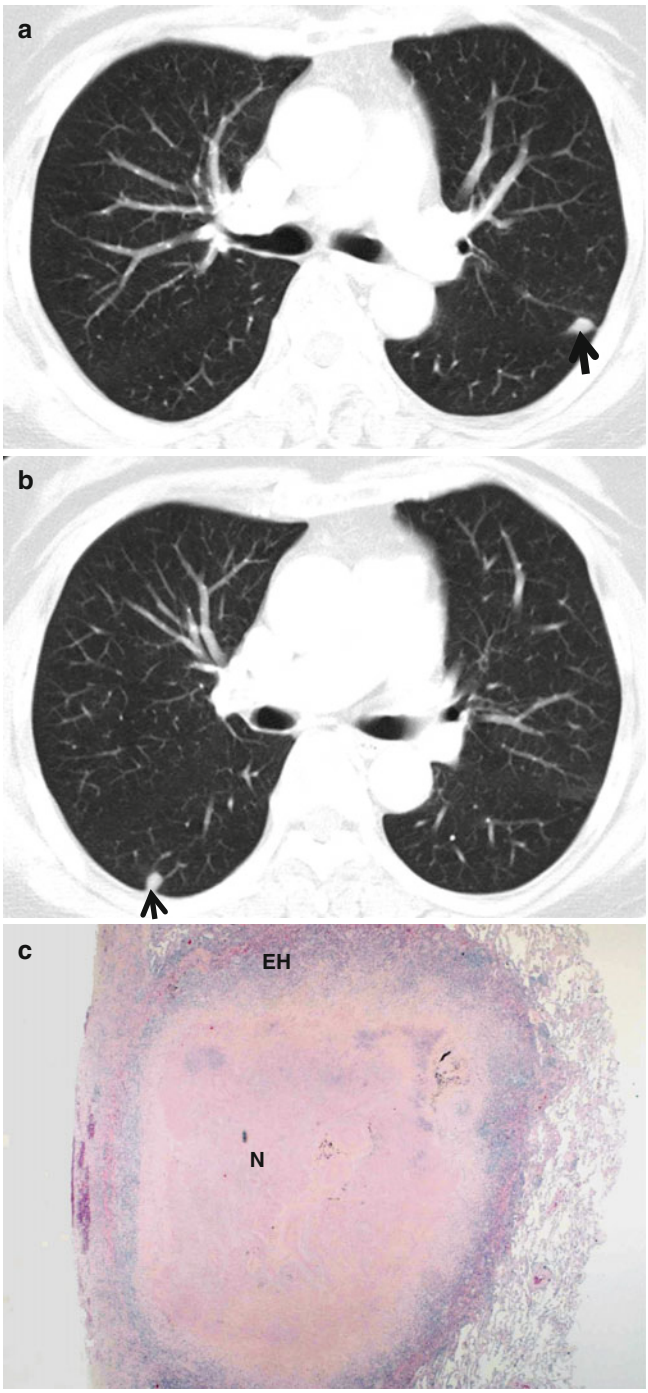

Fig. 1.2 Small nodules representing rheumatoid nodules in a 70-year-old woman with rheumatoid arthritis. (**a**, **b**) CT scans (5.0-mm section thickness) obtained at levels of main bronchi (**a**) and bronchus intermedius (**b**), respectively, show subcentimeter nodules (*arrows*) in the left upper lobe and right lower lobe. (**c**) Low-magnification (×2) photomicrograph of biopsy specimen obtained from right lower lobe nodule demonstrates central necrosis (*N*) area surrounded by a rim of epithelioid histiocytes (*EH*) and fibrous tissue

Key Points for Differential Diagnosis

1. The growth rate of small nodules should be assessed using serial volume measurements rather than diameter. Computer-aided 3D quantitative volume-measurement methods have been developed and applied clinically [4–6].
2. On multivariate analysis, lobulated or spiculated margin and the absence of a satellite nodule appear to be independently associated with malignant nodule with high odd ratio [7].
3. Diffuse, laminated, central nodular, and popcorn-like calcifications within nodules suggest benignity; on the other hand, eccentric or stippled calcifications have been described in malignant nodules [1].
4. Fat or calcification may be observed in up to 30–50 % of pulmonary hamartoma [8].
5. Evaluation based on analyses of wash-in values (>25 HU) plus morphologic features (lobulated or spiculated margin and absence of a satellite nodule) on dynamic CT appears to be the most efficient method for characterizing an SPN [9].
6. By rendering both morphologic and metabolic information, ^{18}fluorine fluorodeoxyglucose (FDG) PET–CT allows significantly better specificity than CT alone or PET alone, and both PET–CT and PET alone provide more confidence than CT alone for the characterization of SPNs [10]. But due to expensive cost and high radiation dose, it may be selectively used to characterize SPNs when dynamic CT shows inconsistent results between morphologic and hemodynamic nodule characteristics [1].
7. Specifically for small nodules less than 10 mm in diameter, serial volume measurements of nodules are regarded as the most reliable technique for their characterization [1].

Lung Cancer (Solid Adenocarcinoma)

Pathology and Pathogenesis

Adenocarcinoma is the most common histologic type of lung cancer in many countries. Adenocarcinoma is a malignant epithelial tumor with glandular differentiation or mucin production, showing lepidic, acinar, papillary, solid, and micropapillary pattern or a mixture of these patterns [11] (Figs. 1.1 and 1.3).

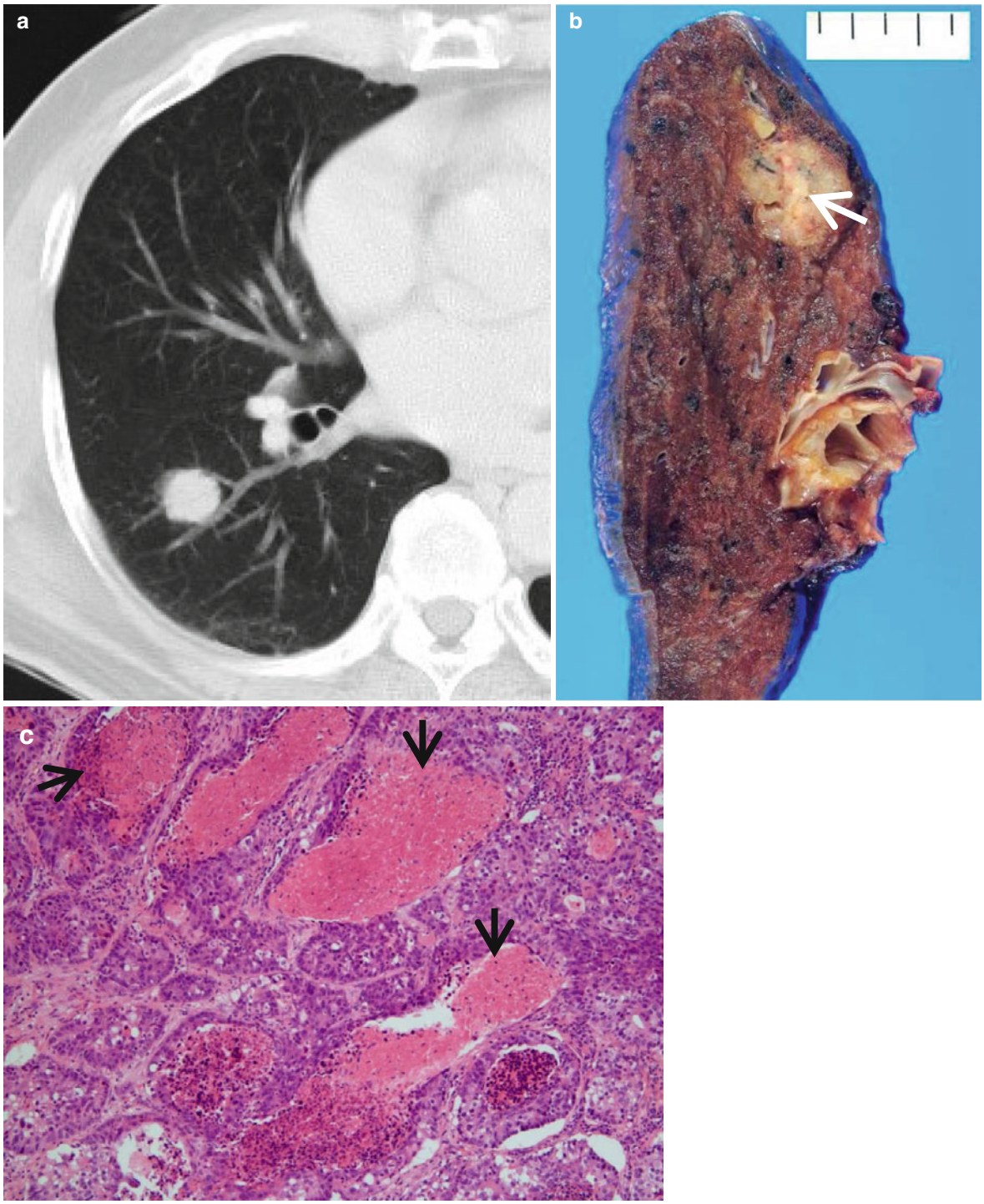

Fig. 1.3 High-grade lung adenocarcinoma simulating a metastatic nodule from a colon cancer in a 65-year-old man. (**a**) CT scan (5.0-mm section thickness) obtained at level of truncus basalis shows a 21-mm-sized nodule in superior segment of the right lower lobe. (**b**) Gross pathologic specimen demonstrates a yellowish-gray round nodule with yellow necrotic spots (*arrow*). (**c**) High-magnification (×200) photomicrograph discloses high-grade, enteric-type lung adenocarcinoma showing glandular structures with multifocal dirty necrosis (*arrows*) simulating metastatic colon adenocarcinoma

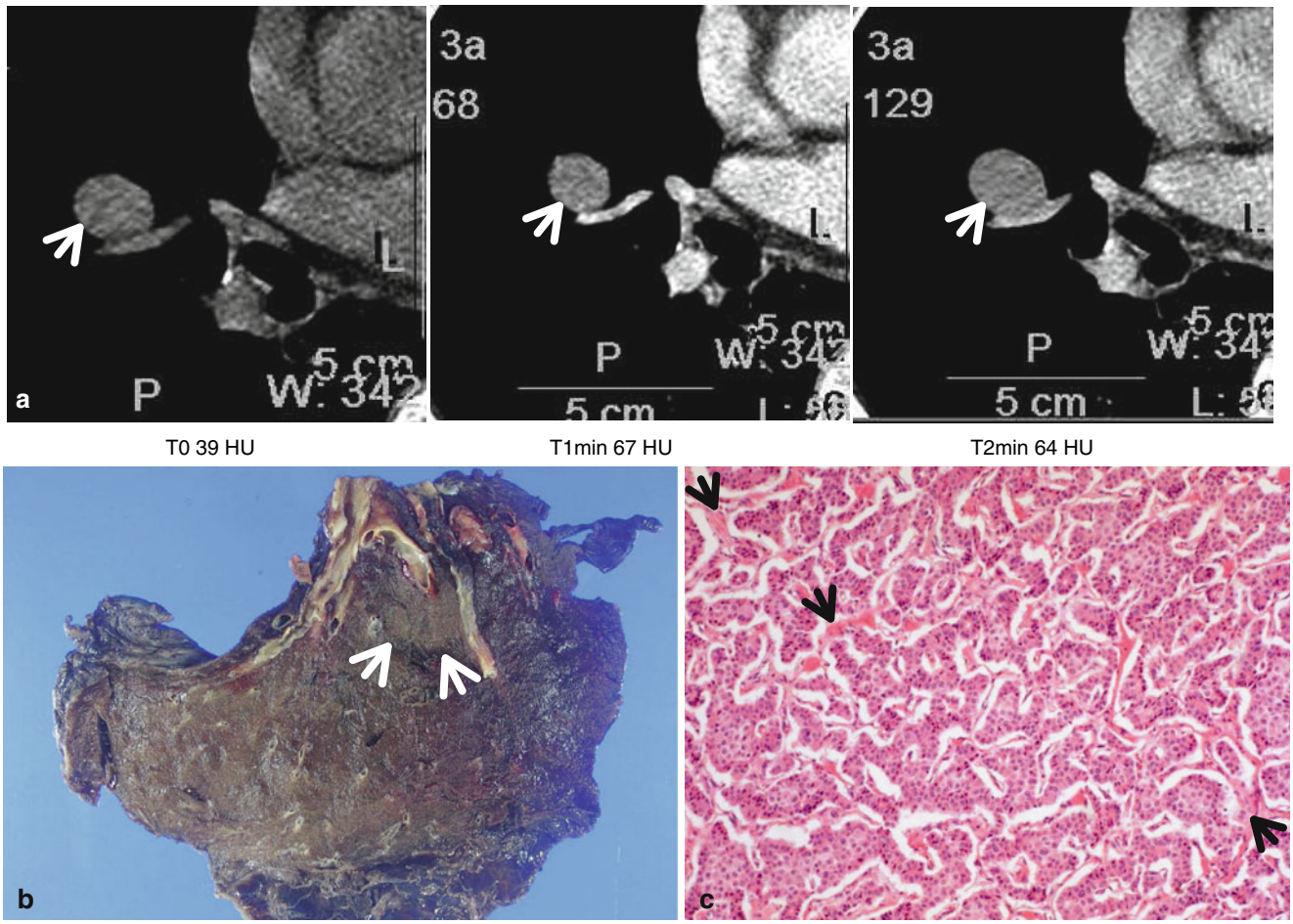

Fig. 1.4 Typical carcinoid tumor showing high and early enhancement in a 58-year-old man. (**a**) Dynamic CT scans obtained at level of right middle lobar bronchus takeoff show an 18-mm-sized well-defined nodule (*arrows*) in the right middle lobe. Nodule depicts high enhancement (39 HU, 67 HU, and 64 HU; before, at 1 min, and at 2 min after contrast-medium injection, respectively). (**b**) Gross pathologic specimen demonstrates a well-defined nodule (*arrows*) in the right middle lobe adjacent to the segmental bronchus. (**c**) High-magnification (×100) photomicrograph of right lower lobectomy specimen discloses neoplastic cells grouped in small nests separated by numerous thin-walled vascular stroma (*arrows*)

Symptoms and Signs

Patients with lung cancer presenting with an SPN are usually asymptomatic. Physical examination shows no specific abnormality. In most cases, the SPN is detected by routine chest imaging.

CT Findings

The characteristic CT finding of solid adenocarcinoma consists of a solitary nodule or mass with a lobulated or spiculated margin. On multivariate analysis, lobulated or spiculated margin and the absence of a satellite nodule appear to be independently associated with malignant nodule with high odd ratio [7]. The nodules enhance following intravenous administration of contrast medium. The enhancement of >25 HU plus morphologic malignant features on dynamic CT appears to be the most efficient method for characterizing a malignant SPN [9].

CT–Pathology Comparisons

The histopathologic correlation of spiculated margin is variable and may correspond to the strands of fibrous tissue that extend from the tumor margin into the lung, to the direct infiltration of tumor into the adjacent parenchyma, to the

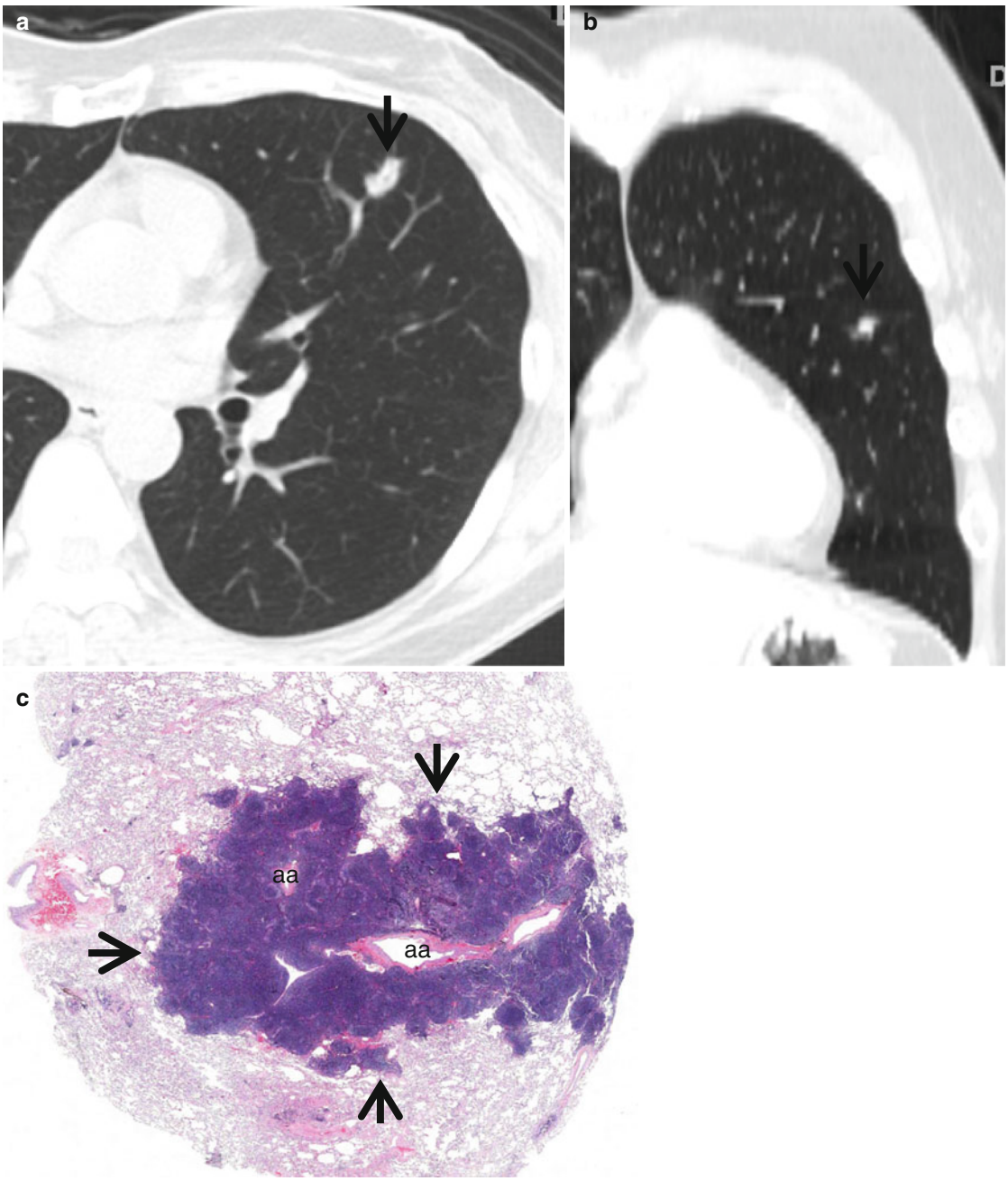

Fig. 1.5 Bronchus-associated lymphoid tissue (BALT) lymphoma in a 51-year-old woman. (**a**, **b**) Transverse (**a**, 2.5-mm section thickness) and coronal reformatted (**b**) CT scans, respectively, show a 13-mm-sized polygonal nodule (*arrows*) in lingular division of the left upper lobe. Lesion has internal CT air-bronchogram sign. (**c**) Low-magnification (×2) photomicrograph of biopsy specimen obtained from left upper lobe nodule demonstrates lymphoepithelial lesions (*arrows*) surrounding the pulmonary arteries (*aa*) and their accompanying bronchi (lumina have been compressed and collapsed)

small foci of parenchymal collapse as a result of bronchiolar obstruction by the expanding tumor, or to the spread of tumor cells into the lymphatic channels and interstitial tissue of adjacent vessels, airways, or the interlobular septa [12]. The enhancement of nodules presumably reflects the vascular stroma of the tumor [13].

Patient Prognosis

In solitary adenocarcinomas with part-solid and solid nodule, the prognosis depends on nodal and distant metastasis. Solid tumors exhibit more malignant behavior and have a poorer prognosis than part-solid tumors [14].

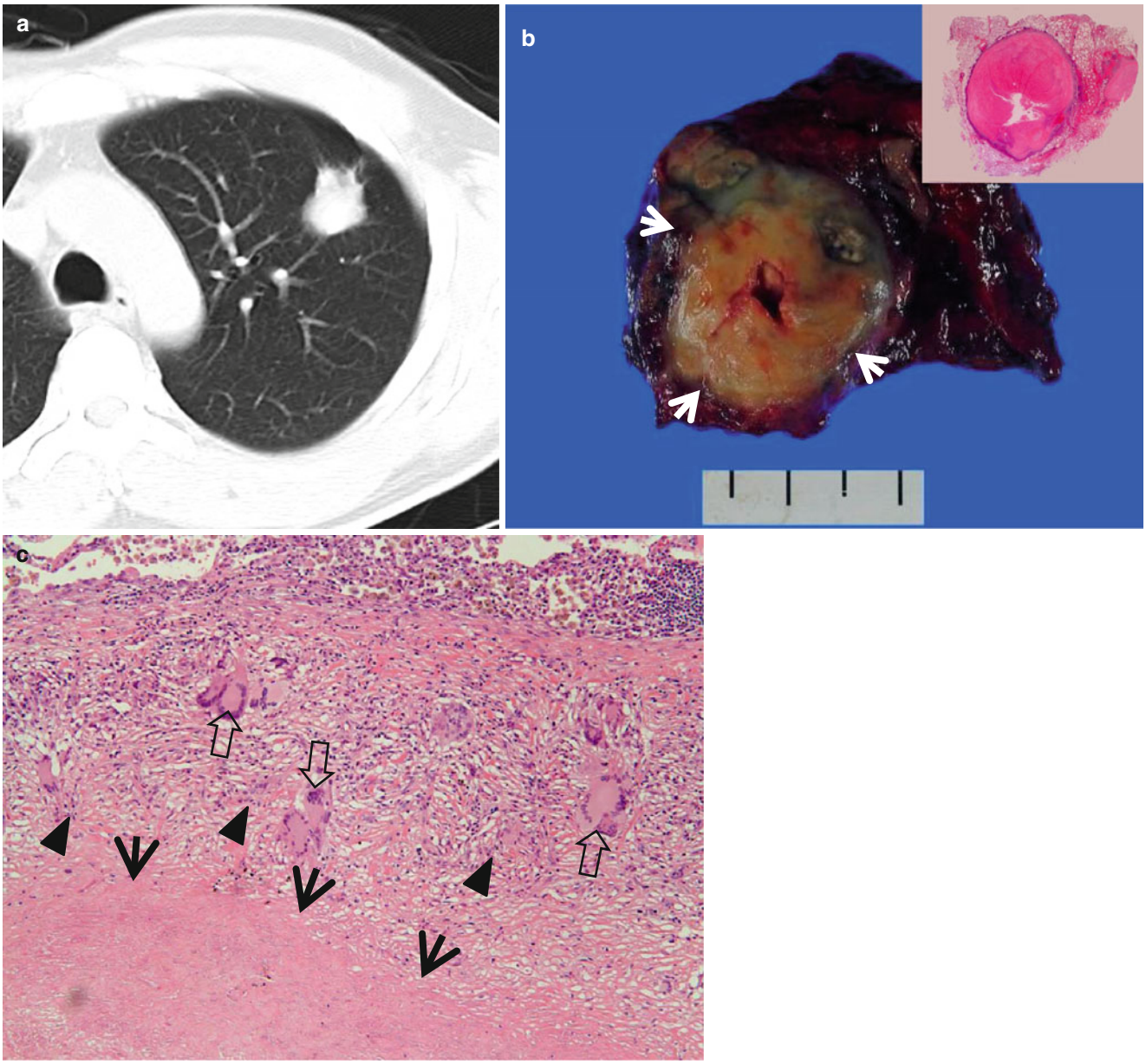

Fig. 1.6 Tuberculoma in a 47-year-old woman. (**a**) CT scan (5.0-mm section thickness) obtained at level of aortic arch shows a 27-mm-sized nodule in anterior segment of the left upper lobe. (**b**) Gross pathologic specimen demonstrates a well-defined round nodule (*arrows*). *Inset*: central caseation necrosis and peripheral epithelioid histiocytes, multinuclear giant cells, and collagenous tissue. (**c**) High-magnification (×100) photomicrograph discloses a focus of a necrotic lung (*arrows*) surrounded by a layer of epithelioid histiocytes (*arrowheads*) and scattered giant cells (*open arrows*). Numerous lymphocytes and collagenous tissues are seen adjacent to granulomatous inflammation

Carcinoid or Atypical Carcinoid

Pathology and Pathogenesis

Carcinoids are slow-growing neuroendocrine tumors characterized by their growth patterns (organoid, trabecular, insular, palisading, ribbon, rosette-like arrangements). They consist of typical carcinoids and atypical carcinoids according to mitotic count or presence of necrosis. Carcinoid is a distinct disease entity, discriminated from other pulmonary neuroendocrine tumors such as large cell neuroendocrine carcinoma or small cell carcinoma [15] (Fig. 1.4).

Symptoms and Signs

Typical carcinoid may be accompanied with hormone-related manifestations. Fewer than 5 % have the carcinoid syndrome (cutaneous flushing, bronchospasm, diarrhea). Cushing's syndrome can also occur. Atypical carcinoid, one

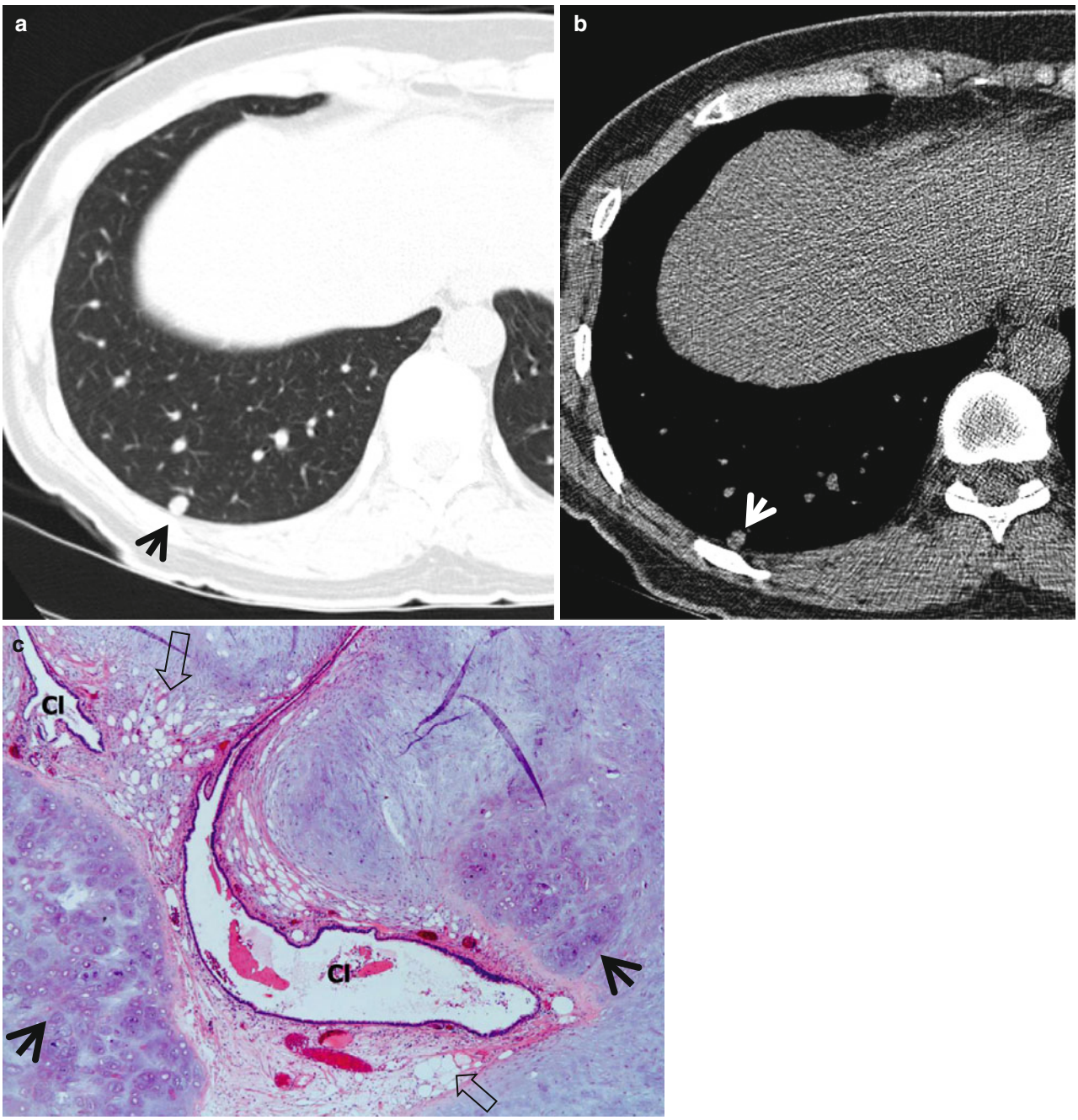

Fig. 1.7 Chondroid hamartoma in a 40-year-old woman. (**a**, **b**) Lung (**a**) and mediastinal (**b**) window images of CT scan (5.0-mm section thickness) obtained at level of lover dome show an 8-mm-sized well-defined nodule (*arrows*) in posterior basal segment of the right lower lobe. Please note fat and calcification attenuation areas within nodule. (**c**) Low-magnification (×10) photomicrograph of wedge resection from the right lower lobe demonstrates islands of mature chondroid (*arrows*) and adipocytic (*open arrows*) tissues. Also note entrapped bronchiolar epithelial cleft (*Cl*) within lesion

on the contrary, may cause lymph node and distant metastasis in half of the cases.

CT Findings

The most common imaging finding of carcinoid is a lung nodule or a mass. The CT features of a peripheral carcinoid presenting as SPN include a lobulated nodule of high attenuation on contrast-enhanced CT; nodule that densely enhances with IV contrast-medium administration; the presence of calcification (approximately 30 % of cases have calcification on CT) (Fig. 1.4); subsegmental airway involvement on thin-section analysis; and nodules associated with distal hyperlucency, bronchiectasis, or atelectasis [16]. Typical carcinoid tends to be smaller (average diameter 2 cm) than atypical

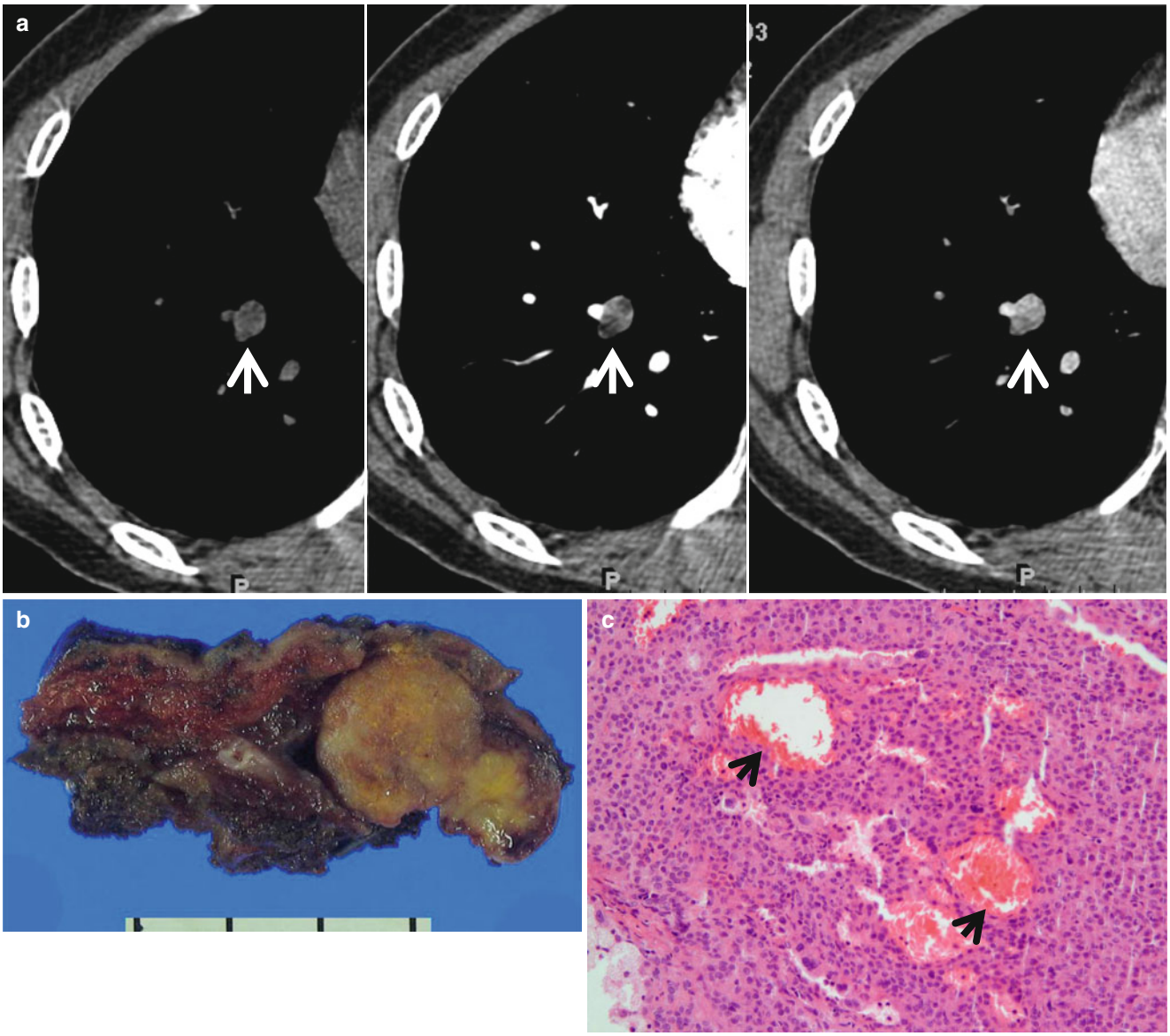

Fig. 1.8 Sclerosing pneumocytoma (hemangiomas) showing high and early enhancement in a 50-year-old woman. (**a**) Dynamic CT scans obtained at level of suprahepatic inferior vena cava (IVC) show a 16-mm-sized well-defined nodule (*arrows*) in the right lower lobe. Nodule depicts high enhancement (19 HU, 38 HU, and 69 HU; before, at 1 min, and at 2 min after contrast-medium injection, respectively). (**b**) Gross pathologic specimen obtained with wedge tumor resection demonstrates a well-defined yellowish round nodule. (**c**) High-magnification (×200) photomicrograph discloses solid growth of polygonal cells with internal hemorrhagic spaces (*arrows*)

carcinoid (average diameter 4 cm) [17]. Secondary effects on distal lung parenchyma such as distal hyperlucency are uncommon in atypical carcinoids.

CT–Pathology Comparisons

The neoplastic cells of carcinoids are grouped in small nests or trabeculae separated by a prominent vascular stroma (Fig. 1.4). Because of their vascular stroma, most carcinoids show marked enhancement following intravenous administration of contrast [18]. Segmental or lobar atelectasis, obstructive pneumonitis, and segmental oligemia are related to complete or partial obstruction of airway.

Patient Prognosis

Since typical carcinoids are extremely slow growing, the long-term prognosis is excellent if completely resected.

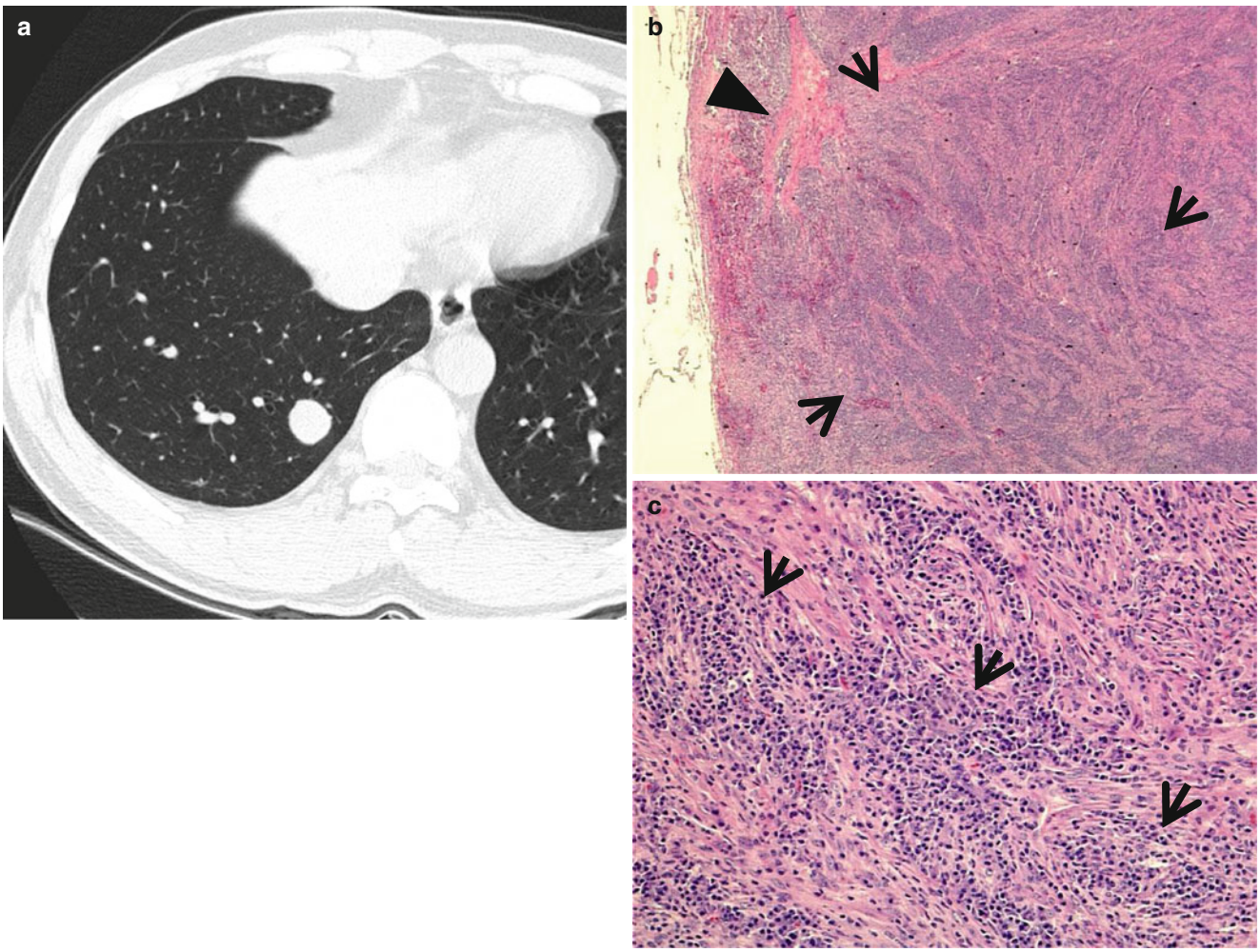

Fig. 1.9 Inflammatory myofibroblastic tumor in a 29-year-old man. (**a**) Thin-section (2.5-mm section thickness) CT scan obtained at level of suprahepatic inferior vena cava (IVC) shows a 19-mm-sized well-defined nodule in the right lower lobe. (**b**) Low-magnification (×2) photomicrograph of wedge resection of tumor from the right lower lobe demonstrates areas of inflammatory cell infiltration (*arrows*; mainly composed of plasma cells) and fibrosis (*arrowhead*). (**c**) High-magnification (×100) photomicrograph discloses fascicular spindle cell proliferation and admixed areas of lymphocytes and plasma cells (*arrows*)

However, all carcinoids are malignant although indolent. Nodal involvement clearly affects survival [19]. The 5-year survival of patients with atypical carcinoids is only 57 %.

BALT Lymphoma

Pathology and Pathogenesis

Pulmonary marginal zone B-cell lymphoma of bronchus-associated lymphoid tissue (BALT) is an extranodal lymphoma, which is thought to arise in acquired MALT secondary to inflammatory or autoimmune processes. The neoplastic cells infiltrate the bronchiolar epithelium, forming lymphoepithelial lesion [20] (Fig. 1.5).

Symptoms and Signs

BALT lymphoma of SPN rarely causes pulmonary symptoms. Weight loss and night sweating may be found. Extrapulmonary symptoms and signs of connective tissue diseases such as Sjögren's syndrome, systemic lupus erythematosus, and rheumatoid arthritis may occur.

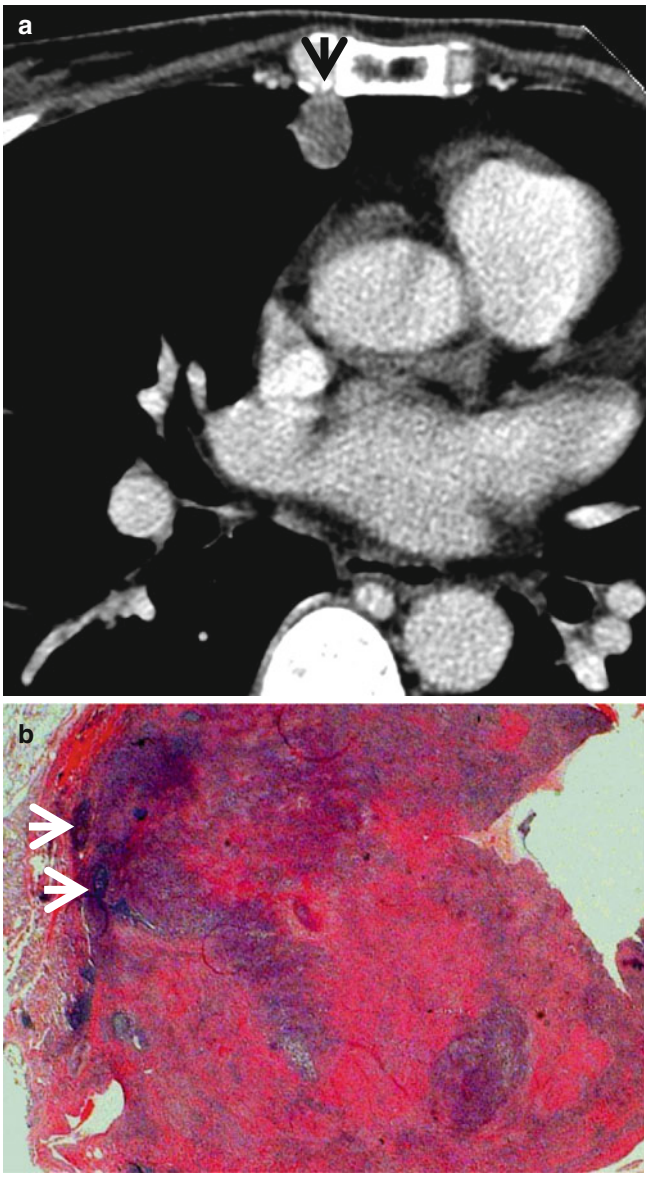

Fig. 1.10 ANCA (antineutrophil cytoplasmic antibody)-associated granulomatous vasculitis (former Wegener's granulomatosis) manifesting as a solitary pulmonary nodule in a 51-year-old woman. (**a**) Mediastinal window image of CT scan (5.0-mm section thickness) obtained at level of the right middle lobar bronchus shows a 13-mm-sized nodule (*arrow*) in the right middle lobe. (**b**) Low-magnification (×40) photomicrograph of wedge resection of tumor from the right middle lobe demonstrates basophilic inflammatory nodule containing geographic necrotic areas (*arrows*)

CT Findings

Typical CT findings of BALT lymphoma include solitary (Fig. 1.5) or multifocal nodules or masses and areas of airspace consolidation with an air bronchogram [20, 21]. Less common findings include ground-glass opacity (GGO) lesion, interlobular septal thickening, centrilobular nodules, and bronchial wall thickening and pleural effusion.

Table 1.1 Common diseases manifesting as solitary pulmonary nodule

Disease	Key points for differential diagnosis
Malignant nodule	
Lung cancer	Wash-in values of >25 HU, lobulated or spiculated margin, and absence of a satellite nodule
Carcinoid	Lobulated nodule with dense enhancement
BALT lymphoma	Consolidation or nodules with air bronchograms
Solitary metastasis	
Benign nodule	
Granuloma	No or little enhancement, satellite nodules
Hamartoma	Focal areas of fat or calcification, septal or cleft-like enhancement
Sclerosing hemangioma	Subpleural homogeneous mass, rapid and strong enhancement
Inflammatory myofibroblastic tumor	
Rheumatoid nodule	
Parasitic infection (PW)	Cavitary nodules or masses in the subpleural or subfissural areas
ANCA-associated granulomatous vasculitis	Multiple, bilateral, subpleural nodules or masses

Note: *HU* Hounsfield unit, *BALT* bronchus-associated lymphoid tissue, *PW* *Paragonimus westermani*, *ANCA* antineutrophil cytoplasmic antibody

CT–Pathology Comparisons

CT findings of BALT lymphoma showing solitary or multifocal nodules or masses and areas of airspace consolidation are related to proliferation of tumor cells within the interstitium such that the alveolar airspaces and transitional airways are obliterated [22] (Fig. 1.5). Because the bronchi and membranous bronchioles tend to be unaffected, an air bronchogram is common. Interlobular septal thickening, centrilobular nodules, and bronchial wall thickening on CT images are related to perilymphatic interstitial infiltration of tumor cells.

Patient Prognosis

BALT lymphoma shows the indolent clinical course. The estimated 5- and 10-year overall survival rates have been reported to be 90 and 72 %, respectively [23]. Age and performance status are the prognostic factors.

Tuberculoma

Pathology and Pathogenesis

Tuberculoma is a parenchymal nodular histologic reaction which is primarily granulomatous and necrotizing with frequent cavitation. The granulomas may have palisading histiocytes, prominent epithelioid cells, or Langerhans-type giant cells. These necrotizing granulomas can progress to fibrosis and calcification [24] (Fig. 1.6).

Symptoms and Signs

In active tuberculoma, constitutional symptoms (fever, malaise, night sweating, weight loss, and anorexia) as well as respiratory symptoms (cough, blood-tinged sputum) occur infrequently. Most patients with inactive tuberculoma are asymptomatic.

CT Findings

Tuberculoma is seen as a sharply marginated round or oval lesion measuring 0.5–4.0 cm in diameter [10, 25]. However, fibrosis related to vessels, interlobular septa, or lung parenchyma adjacent to the nodule may result in a spiculated margin. Calcification within the nodule is present in 20–30 % of cases. Satellite nodules around the tuberculoma may present in as many as 80 % of cases [26]. Following intravenous administration of contrast medium, tuberculomas usually show no or little enhancement although sometimes show ringlike enhancement [27] (Fig. 1.6).

CT–Pathology Comparisons

The central part of tuberculoma consists of caseous material and the periphery of epithelioid histiocytes and multinucleated giant cells and a variable amount of collagen. Ringlike enhancement corresponds histologically to the granulomatous inflammatory tissue capsule, whereas the non-enhancing area corresponds to the central necrotic material [27].

Patient Prognosis

It has been reported that a majority of pulmonary tuberculomas show decrease in size with antituberculous treatment. Over 15 % did not show a decrease in size even after the medical treatment [28].

Hamartoma

Pathology and Pathogenesis

Hamartomas are benign neoplasms composed of varying proportions of mesenchymal tissues, such as cartilage, fat, smooth muscle, and connective tissue, typically combined with entrapped respiratory epithelium. Genetic studies indicate a neoplastic rather than hamartomatous origin [29] (Fig. 1.7).

Symptoms and Signs

Pulmonary hamartomas are usually asymptomatic and found incidentally when imaging the chest for other reasons. It can occasionally present with hemoptysis, bronchial obstruction, and cough (especially endobronchial types) [30].

CT Findings

The characteristic CT findings of hamartomas are comprised of a lesion of 2.5 cm or smaller in diameter, of a smooth margin, and of focal areas of fat (CT attenuation values between −40 and −120 HU) or calcification [8]. However, these findings are present in only 30–50 % of the tumors (Fig. 1.7). Recent MRI and dynamic CT studies demonstrate septal or cleft-like enhancements of pulmonary hamartomas [31, 32].

CT–Pathology Comparisons

Hamartomas are composed of mature cartilage and fat, which are often surrounded by a thin layer of loose mesenchymal tissue. Recent MRI and dynamic CT studies demonstrated septal or cleft-like enhancement of pulmonary hamartomas [31, 32]. Pathologically, these structures were found to represent variable mesenchymal tissue components arrayed along respiratory epithelial cells lining the cleft and show richer vascularity than main cartilaginous portion of pulmonary hamartoma.

Patient Prognosis

Surgical resection is curative. Recurrence or malignant transformation is rare.

Sclerosing Hemangioma

Pathology and Pathogenesis

Although sclerosing hemangiomas (SHs) were originally termed as a variant of hemangiomas, now there is a consensus that they are epithelial tumors. SH comprises a mixture of four histologic patterns, such as papillary, sclerotic, solid, and hemorrhagic [33] (Fig. 1.8).

Symptoms and Signs

Most patients are asymptomatic at the time of diagnosis.

CT Findings

On CT scans, SH appears as a well-defined, round- or oval-shaped, homogeneous mass with smooth margin in subpleural area [34]. On dynamic CT, it has strong and rapid enhancement [35] (Fig. 1.8). Unusual manifestations of SH include mediastinal mass, tumor with a cystic appearance, air trapping around the tumor, multiple tumors, or a tumor surrounded by multiple daughter nodules in the same lobe; it can also be accompanied by hilar lymph node metastasis [36–40].

CT–Pathology Comparisons

On CT–pathology comparisons, dynamic characteristics of sclerosing hemangioma depend on the levels of hemangiomatous or papillary (early and strong enhancement) and solid or sclerotic (slow and persistent enhancement and little washout) components present [35] (Fig. 1.8).

Patient Prognosis

Regardless of surgical resection, the prognosis of patients with sclerosing hemangioma is excellent in cases manifesting as SPN.

Inflammatory Myofibroblastic Tumor

Pathology and Pathogenesis

Inflammatory myofibroblastic tumor (IMT) is a proliferation of cells showing myofibroblastic differentiation, and IMT is a subgroup of the broad category of inflammatory pseudotumors and is composed of a variable mixture of collagen, inflammatory cells, and bland spindle cells showing myofibroblastic differentiation [41] (Fig. 1.9).

Symptoms and Signs

Most patients are asymptomatic.

CT Findings

On CT, IMT usually is seen as a well-circumscribed, solitary, peripheral pulmonary nodule or mass with a variable degree of contrast enhancement [41, 42] (Fig. 1.9). The lesion may be homogeneous or heterogeneous after contrast enhancement. Intratumoral calcification has been identified in about 15 % of cases. Endoluminal airway involvement has been known to occur in 10–80 % cases.

CT–Pathology Comparisons

According to the recent theory on the pathogenesis of IMT, the tumor appears to originate from fibroblasts in the connective tissue of the airway [43]. In one series on the studies of CT–pathology correlation of IMT, a much higher incidence of airway involvement (80 %) was noted [41]. Peripheral solitary nodules seen on CT were also related to an adjacent bronchiole on histopathologic examinations (Fig. 1.9). Therefore, when a well-defined polypoid endobronchial nodule or a well-defined peripheral SPN related to an adjacent airway is seen on CT, IMT should be included in the differential diagnosis.

Patient Prognosis

Since incomplete resection is related to a substantial risk of recurrence and locally aggressive behavior, complete surgical resection is the only treatment to prevent recurrence.

ANCA-Associated Granulomatous Vasculitis (Former Wegener's Granulomatosis) Manifesting as a Solitary Pulmonary Nodule

Pathology and Pathogenesis

The classic pattern of pulmonary involvement of ANCA-associated granulomatous vasculitis is that of multiple nodules with frequent cavitation. Solid nodular zones of consolidation with foci of punctate or geographic necrosis, associated with granulomatous inflammation and vasculitis, are often seen [44] (Fig. 1.10).

Symptoms and Signs

When detected as SPN, systemic symptoms are usually absent. Patients may have cough or blood-tinged sputum.

CT Findings

The most common pattern on CT images at the initial presentation is the presence of nodules or masses in 90 % of cases [45] (Fig. 1.10). The distribution of nodules or masses seen on CT is multiple in 85 % of patients, bilateral in 67 %, subpleural in 89 %, and peribronchovascular in 41 %. Airway involvements are also common with segmental or subsegmental bronchial wall thickening in 70 % of patients and large airway abnormality in 30 % of patients. Another common manifestation is airspace consolidation and GGO with random or patchy distribution, seen in 25–50 % of cases. Centrilobular nodules and a tree-in-bud sign pattern may be seen in up to 10 % of patients, usually mixed with other changes.

CT–Pathology Comparisons

The most common imaging findings of pulmonary involvement of ANCA-associated granulomatous vasculitis are multiple bilateral pulmonary nodules with frequent cavitation which are histologically corresponded to large areas of parenchymal necrosis, granulomatous inflammation, and vasculitis [45]. Airspace consolidation and GGO with random or patchy distribution are regarded to diffuse alveolar hemorrhage caused by necrotizing capillaritis. Centrilobular nodules and the tree-in-bud sign may result from bronchiolar inflammatory changes rather than from vasculitis.

Patient Prognosis

Solitary nodular form of ANCA-associated granulomatous vasculitis may have a better prognosis [46]. With the introduction of the use of cyclophosphamide in immunosuppressive therapy, complete remission has been achieved in 70–90 % of patients, but relapses are common. A poor prognosis is associated with DAH, severe azotemia, an advanced age, and positivity for proteinase 3 ANCA [47].

Ground-Glass Opacity Nodule

Definition

Ground-glass opacity nodules (GGNs, or subsolid nodules) are further divided into nonsolid pure GGNs and part-solid nodules; the former nodules have no patch of parenchyma that are completely obscured with soft tissue structures (Fig. 1.11), whereas the latter nodules harbor such patches [48, 49] (Fig. 1.12).

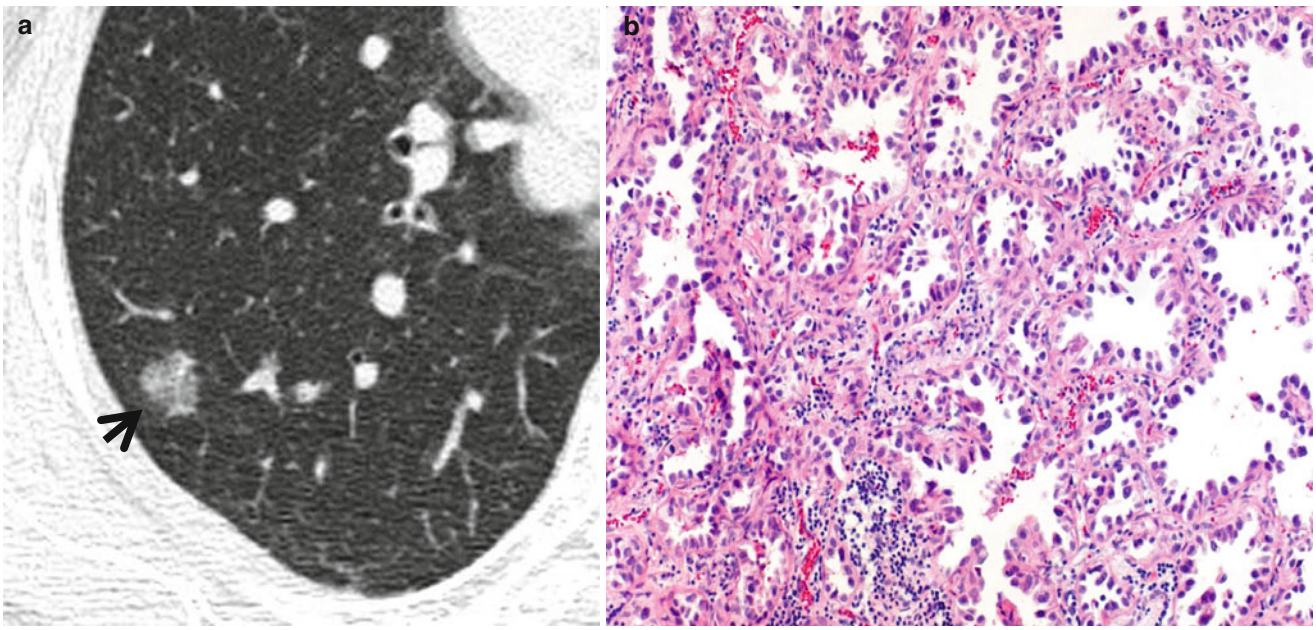

Fig. 1.11 Pure ground-glass opacity nodule representing adenocarcinoma in situ (AIS, former bronchioloalveolar carcinoma) in a 45-year-old woman. (**a**) Targeted view of thin-section (1.5-mm section thickness) CT scan obtained at the basal segmental bronchi shows a 13-mm-sized ground-glass opacity nodule (*arrow*) in superior segment of the right lower lobe. (**b**) High-magnification photomicrograph shows spread of neoplastic cells on airspace surface with preservation of underlying architecture (so-called lepidic growth). Note thickened alveolar walls

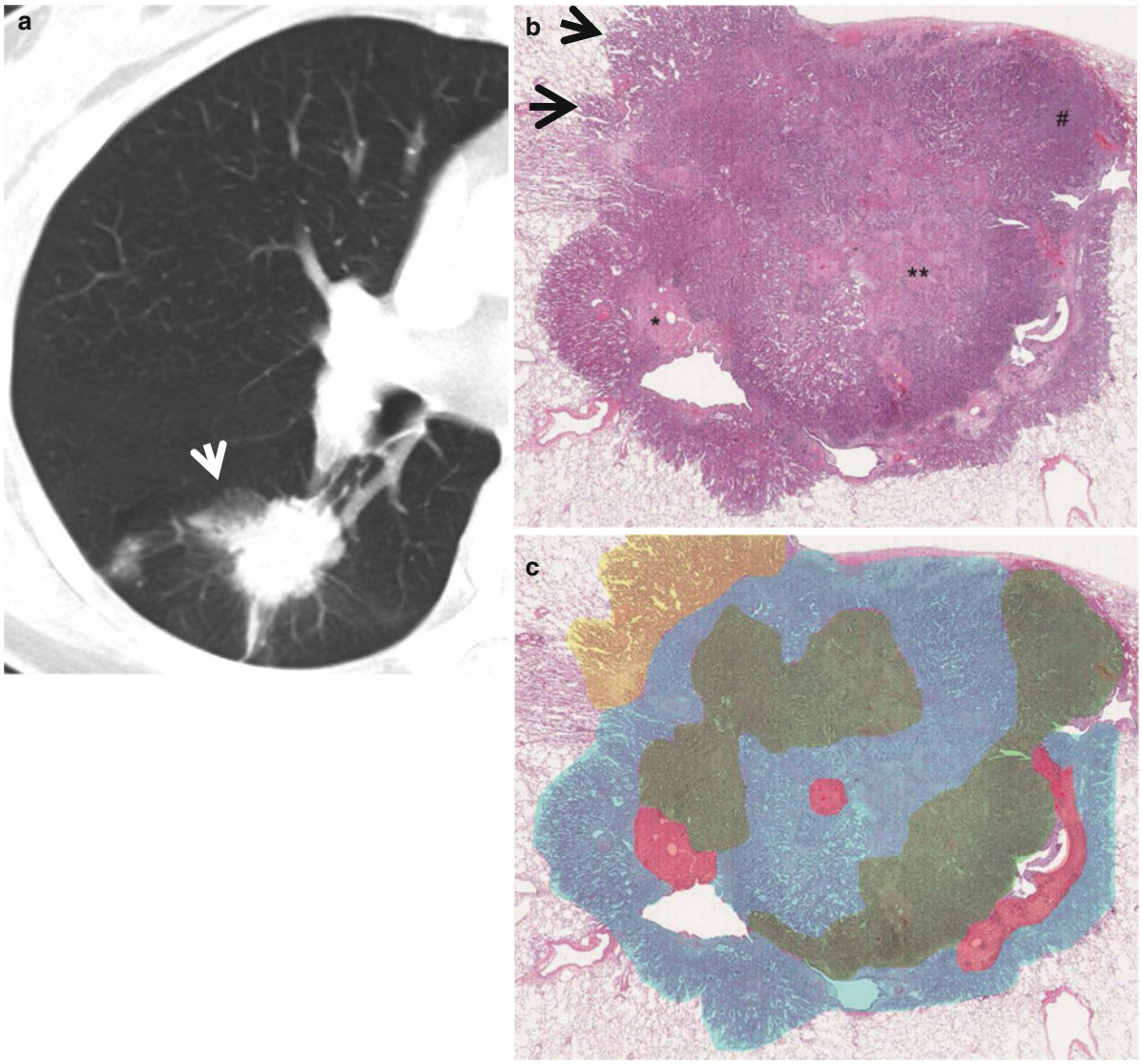

Fig. 1.12 A part-solid nodule representing lung adenocarcinoma in a 67-year-old woman. (**a**) Targeted view of thin-section (2.5-mm section thickness) CT scan obtained at superior segmental bronchus level of the right lower lobe shows a 25-mm-sized part-solid nodule (*arrow*) in superior segment of the right lower lobe. (**b**) Low-magnification (×10) photomicrograph (H & E stain) demonstrates internal scar tissue (*), surrounding areas of acinar (**) and solid (#) adenocarcinoma patterns, and lepidic pattern (*arrows*, uniform cuboid cellular proliferation along alveolar walls) only at tumor periphery. (**c**) In a schematic drawing of tumor components, percentages of lepidic growth pattern (*yellow area*), acinar pattern (*blue area*), solid pattern (*green area*), and central fibrosis (*red area*) are estimated as 10, 50, 30, and 10 %, respectively (Reprinted from Lee et al. [70] with permission)

Diseases Causing the Pattern

The persistent presence of a GGN at thin-section CT (TSCT), in more than 80 % of cases, suggests the diagnosis of *atypical adenomatous hyperplasia* (*AAH*), *adenocarcinoma in situ* (*AIS*), *minimally invasive adenocarcinoma* (*MIA*), or invasive lung adenocarcinomas [48]. AAH and AIS are collectively called preinvasive adenocarcinoma [11] (Figs. 1.13 and 1.14). Among lung cancer screening-detected nodules, malignancy rates of GGNs (34 %, subsolid nodules) are higher than that of solid nodules (7 %); in particular, the rates of part-solid nodules and pure GGNs (nonsolid nodules) were 64 and 18 %, respectively [50]. Bronchus-associated lymphoid tissue (BALT) lymphoma may also appear as GGN [20]. Pulmonary non-hemorrhagic or hemorrhagic metastases from extrathoracic malignant melanoma, choriocarcinoma, or renal cell carcinoma may also be seen as a GGN [51].

Subsolid nodules can be seen in nontumorous conditions including *Loeffler's syndrome* (*pulmonary infiltration with eosinophilia* [*PIE*] *syndrome*), invasive pulmonary aspergillosis, and organizing pneumonia [52] (Table 1.2).

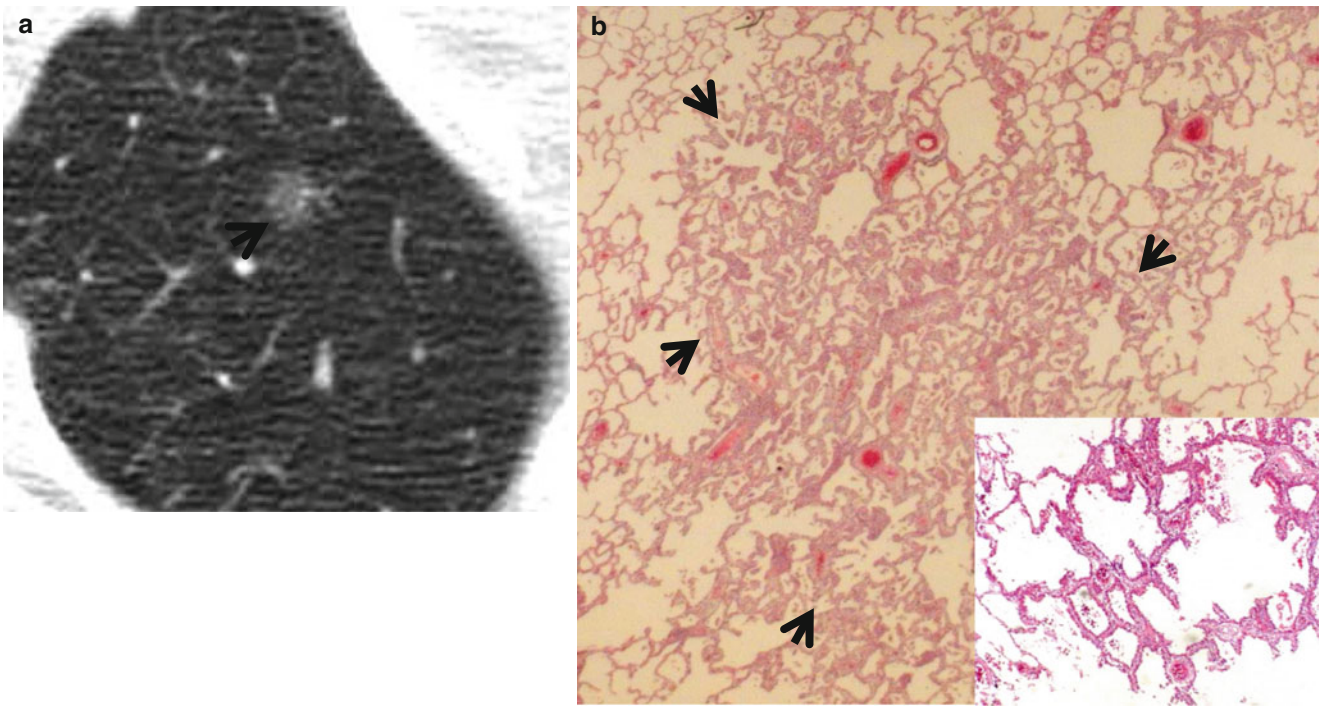

Fig. 1.13 Atypical adenomatous hyperplasia in a 44-year-old man. (**a**) Targeted view of thin-section (2.5-mm section thickness) CT scan obtained throughout the right upper lobe shows a 9-mm-sized ground-glass opacity nodule (*arrow*) in the right upper lobe. (**b**) Low-magnification (×10) photomicrograph (H & E stain) demonstrates atypical epithelial cell proliferation along alveolar septa in atypical adenomatous hyperplasia (*arrows*). *Inset*: no attendant stromal thickening and harbors more airspaces and fewer cellular components histopathologically than adenocarcinoma in situ

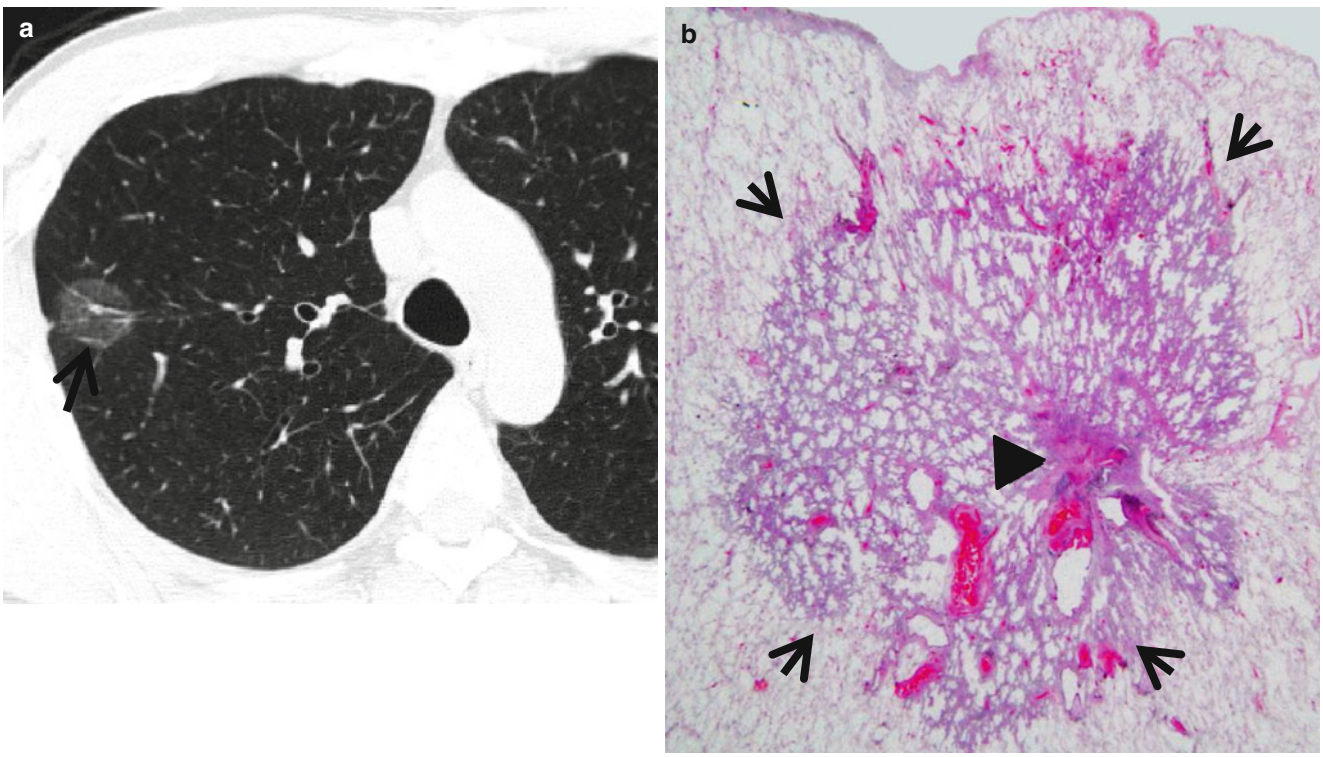

Fig. 1.14 Adenocarcinoma in situ (former bronchioloalveolar carcinoma) in a 56-year-old man. (**a**) Lung window image of thin-section (1.5-mm section thickness) CT scan obtained at level of the azygos arch shows a 19-mm-sized ground-glass opacity nodule (*arrow*) in the right upper lobe. (**b**) Low-magnification (×10) photomicrograph (H & E stain) demonstrates lepidic tumor growth along alveolar walls (*arrows*). Please note maintained alveolar architecture. *Arrowhead* indicates scar tissue within tumor

Distribution

Likelihood ratio for malignancy in upper and middle lobe nodule is 1.22 as compared with 0.66 in lower lobe nodule [3].

Clinical Considerations

Fleeting or transient and migratory nature of GGNs favors the diagnosis of an inflammatory condition such as Loeffler's syndrome, whereas persistent presence suggests the diagnosis of preinvasive, minimally invasive, and invasive lung adenocarcinomas or BALT lymphoma [48, 52].

Table 1.2 Common diseases manifesting as ground-glass opacity nodule

Disease	Key points for differential diagnosis
Tumorous condition	
AAH	Faint pure GGN usually < 5 mm
Nonmucinous AIS	Pure GGN
MIA	Part-solid nodule for nonmucinous MIA, solid or part-solid nodule for mucinous MIA
BALT lymphoma	Consolidation or nodules with air bronchograms
Metastasis from melanoma or RCC	
Nontumorous condition	
Loeffler's syndrome	Transient, migrating periphery GGO or consolidation
Invasive pulmonary aspergillosis	Nodules with a GGO, wedge-shaped pleural-based areas of consolidation
Organizing pneumonia	

Note: *AAH* atypical adenomatous hyperplasia, *AIS* adenocarcinoma in situ, *MIA* minimally invasive adenocarcinoma, *BALT* bronchus-associated lymphoid tissue, *RCC* renal cell carcinoma, *GGN* ground-glass nodule, *GGO* ground-glass opacity

Key Points for Differential Diagnosis

1. New lung adenocarcinoma classifications have been put forth by the International Association for the Study of Lung Cancer/American Thoracic Society/European Respiratory Society. The principal changes are as follows: (1) an end to the use of the term bronchioloalveolar carcinoma (BAC; the term is replaced by adenocarcinoma in situ [AIS]), (2) the addition of a new category of minimally invasive adenocarcinoma (e.g., patients with a 2-cm or smaller AIS with an invasive area measuring ≤5 mm in thickness), (3) elimination of the category of mixed subtype adenocarcinoma, and (4) renaming of what was formerly referred to as mucinous BAC as mucinous adenocarcinoma [11] (Table 1.3).
2. Although the maximum diameter (8 mm ± 3.8) of AAH tended to be smaller than that of AIS or invasive adenocarcinoma with predominantly lepidic pattern (13 mm ± 6.9), there was no significant difference in morphologic findings at TSCT between AAH and AIS or invasive adenocarcinoma [48].
3. According to a study [53], (1) the size >16.4 mm in diameter in pure GGNs is associated with invasive adenocarcinoma and the size is closely correlated with the mass (nodule volume × attenuation) of a nodule, (2) the mass is significantly larger in invasive adenocarcinoma (mean attenuation value, −507 HU) than no (mean attenuation value, −620) or minimally invasive (mean attenuation value, −636 HU) adenocarcinoma in both uni- and multivariate analyses, (3) the presence of air bronchogram favors the diagnosis of invasive adenocarcinomas in univariate analysis and had very close correlation with nodule size, and finally (4) none with pure GGNs had tumor recurrence or metastasis at 3- or 5-year follow-up study.

Table 1.3 IASLC/ATS/ERS classification of lung adenocarcinoma in resection specimens

Preinvasive lesions
Atypical adenomatous hyperplasia
Adenocarcinoma in situ (≤3 cm, former BAC)
Nonmucinous
Mucinous
Mixed mucinous/nonmucinous
Minimally invasive adenocarcinoma (≤3-cm lepidic predominant tumor with ≤5-mm invasion)
Nonmucinous
Mucinous
Mixed mucinous/nonmucinous
Invasive adenocarcinoma
Lepidic predominant (former nonmucinous BAC pattern, with >5-mm invasion)
Acinar predominant
Papillary predominant
Micropapillary predominant
Solid predominant with mucin production
Variants of invasive adenocarcinoma
Invasive mucinous adenocarcinoma (former mucinous BAC)
Colloid
Fetal (low and high grade)
Enteric

Note: *IASLC* International Association for the Study of Lung Cancer, *ATS* American Thoracic Society, *ERS* European Respiratory Society, *BAC* bronchioloalveolar carcinoma

Atypical Adenomatous Hyperplasia (AAH)

Pathology and Pathogenesis

AAH is a localized, small (usually 0.5 cm or less) proliferation of mildly to moderately atypical type II pneumocytes or Clara cells lining alveolar walls and sometimes respiratory bronchioles (Fig. 1.13). There is a continuum of morphologic changes between AAH and AIS. A spectrum of cellularity and atypia occurs in AAH [11].

Symptoms and Signs

Since AAHs are incidentally detected in the lungs resected for adenocarcinoma or by screening chest CT, patients with AAH are asymptomatic.

CT Findings

On CT, AAH is characteristically shown as a small pure ground-glass nodule (GGN) usually measuring <5 mm [54]. However, no significant difference in the maximum diameter of GGN of AAH and AIS on TSCT was found [48]. The ground-glass opacities (GGOs) of AAH observed on TSCT are typically very faint [49]. AAH can be either single or multiple [55].

CT–Pathology Comparisons

AAH generally exhibits no attendant stromal thickening and harbors more airspaces and fewer cellular components histopathologically than AIS. Therefore, the GGOs of AAH observed on TSCT are typically very faint [49].

Patient Prognosis

AAHs have been proposed as possible precursors of peripheral adenocarcinoma although this hypothesis has yet to be confirmed [56].

Adenocarcinoma in Situ (AIS)

Pathology and Pathogenesis

AIS (one of the lesions formerly known as BAC) is a localized small (≤3 cm) adenocarcinoma with growth restricted to neoplastic cells along preexisting alveolar structures (lepidic growth), lacking stromal, vascular, or pleural invasion. Papillary or micropapillary patterns and intra-alveolar tumor cells are absent (Fig. 1.14). AIS is subdivided into nonmucinous and mucinous variants. Virtually, all cases of AIS are nonmucinous [11].

Symptoms and Signs

AIS, owing to its small size and peripheral location, rarely causes symptoms or signs.

CT Findings

On CT, nonmucinous AIS appears typically as a pure GGN. Mucinous AIS can appear as a solid nodule or as a part-solid nodule [57]. Mean maximum diameter of AIS is 13 mm ± 6.9 [48]. The pure GGN of AIS usually appears on TSCT as slightly higher attenuation compared with the very faint GGN of AAH [49]. AIS also can be either single or multiple.

CT–Pathology Comparisons

The GGOs of AIS generally manifest as regions of slightly higher attenuation relative to the very faint opacities of AAH. This difference in GGN attenuation is probably due to histopathologic dissimilarity in the amount of alveolar airspace and cellular components contained within the nodule [58] (Fig. 1.14). The solid or part-solid nodular features of mucinous AIS may be histopathologically related to (1) a prominent central scar, (2) compact tumor cells surrounded by abundant mucin, and (3) alveolar spaces filled with mucin and mononuclear cells and alveolar walls lined with mucin-containing tumor cells [57].

Patient Prognosis

Patients with AIS will have 100 % disease-specific survival if they undergo complete resection [59, 60].

Minimally Invasive Adenocarcinoma (MIA)

Pathology and Pathogenesis

MIA is a small, solitary adenocarcinoma (≤3 cm), with a predominantly lepidic pattern and ≤5-mm invasion in greatest dimension in any one focus (Fig. 1.15). MIA is usually nonmucinous but rarely may be mucinous. MIA is, by definition, solitary and discrete. The criteria for MIA can be applied in the setting of multiple tumors, only if the other tumors are regarded as synchronous primaries rather than intrapulmonary metastases. The invasive component to be

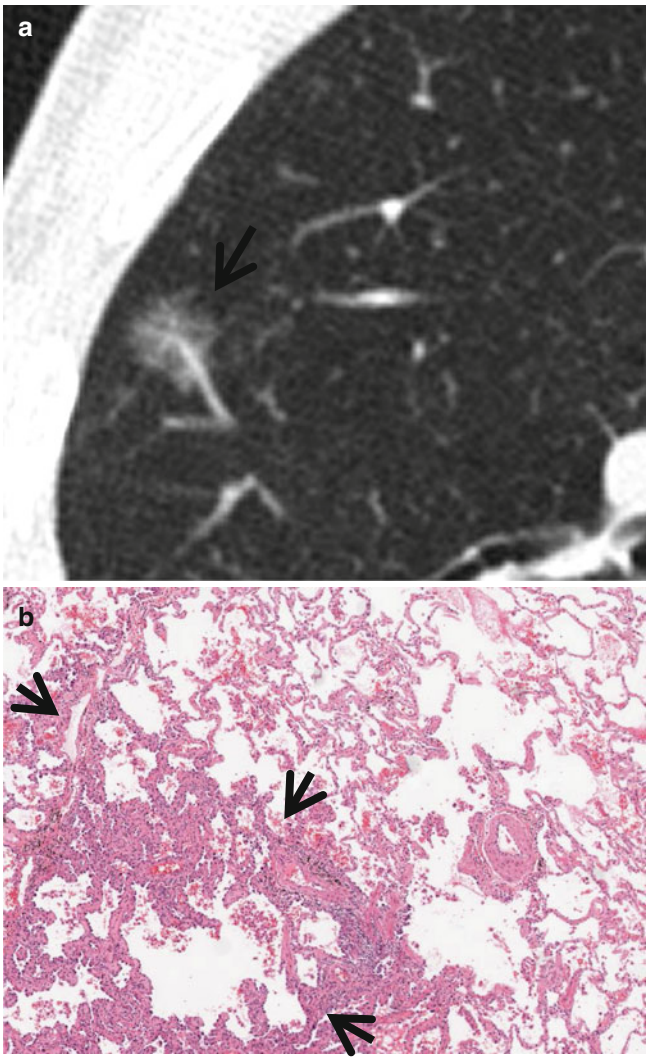

Fig. 1.15 Minimally invasive adenocarcinoma (MIA) in a 64-year-old woman. (**a**) Targeted view of thin-section (2.0-mm section thickness) CT scan obtained throughout the right upper lobe shows a 12-mm-sized ground-glass opacity nodule (*arrow*) in the right upper lobe. (**b**) High-magnification (×100) photomicrograph demonstrates tumor consisting of predominant background lepidic subtype and mixed area (*arrows*) of invasive acinar subtype (less than 5 mm in thickness, thus so-called minimally invasive adenocarcinoma)

measured in MIA is defined as histologic subtypes other than a lepidic pattern or tumor cells infiltrating myofibroblastic stroma. MIA is excluded if the tumor invades lymphatics, blood vessels, or pleura or contains tumor necrosis. If multiple microinvasive areas are found in one tumor, the size of the largest invasive area should be measured in the largest dimension, and it should be ≤5 mm in size [61].

Symptoms and Signs

As in the case of AIS, patients with MIA are usually asymptomatic.

CT Findings

Imaging features of MIA are as yet not fully described. A provisional description of nonmucinous MIA on TSCT is a part-solid nodule consisting of a predominant ground-glass component and a small solid component measuring 5 mm or less [61, 62]. Mucinous MIA can appear as a solid or part-solid nodule [63]. MIA is, by definition, solitary and discrete. For nonsolid nodules, shape does not appear to be a differentiating criterion between AIS and MIA.

CT–Pathology Comparisons

Invasive component of MIA has been thought to be characteristically solid at CT, and the noninvasive lepidic component is hazy and nonsolid (GGO) at thin-section CT [64]. Because the histopathologic components of small adenocarcinomas can include alveolar collapse, inflammatory cells, fibroblasts, fibrosis, as well as invasive adenocarcinoma, the size of the solid component may be larger at CT than the size of the actual invasive adenocarcinoma component [62]. However, because the invasive component in MIA is defined histopathologically [11], the invasive component (≤5 mm in its greatest dimension) does not contribute much to increase CT attenuation and appears as a pure GGN of 10 mm or greater in diameter, not differently from AIS or invasive adenocarcinoma of greater than 16.4 mm in diameter [53]. For the mucinous MIA, the mucin may contribute to a solid or part-solid appearance of tumor at CT.

Patient Prognosis

Patients with nonmucinous MIA (predominantly lepidic growth pattern and invasive components of acinar, papillary, or micropapillary pattern) have shown near 100 % disease-specific or very favorable overall survival, if completely resected [65–67]. There is very limited data regarding mucinous MIA. A recent series of surgically resected solitary mucinous BAC in eight patients had 100 % overall 5-year survival rates [68].

Loeffler's Syndrome

Pathology and Pathogenesis

The lung in Loeffler's syndrome shows intra-alveolar eosinophils and macrophages with proteinaceous exudate. Charcot–Leyden crystals, interstitial eosinophilic infiltrate, organizing pneumonia, or eosinophilic microabscess or granuloma may be present [69] (Fig. 1.16).

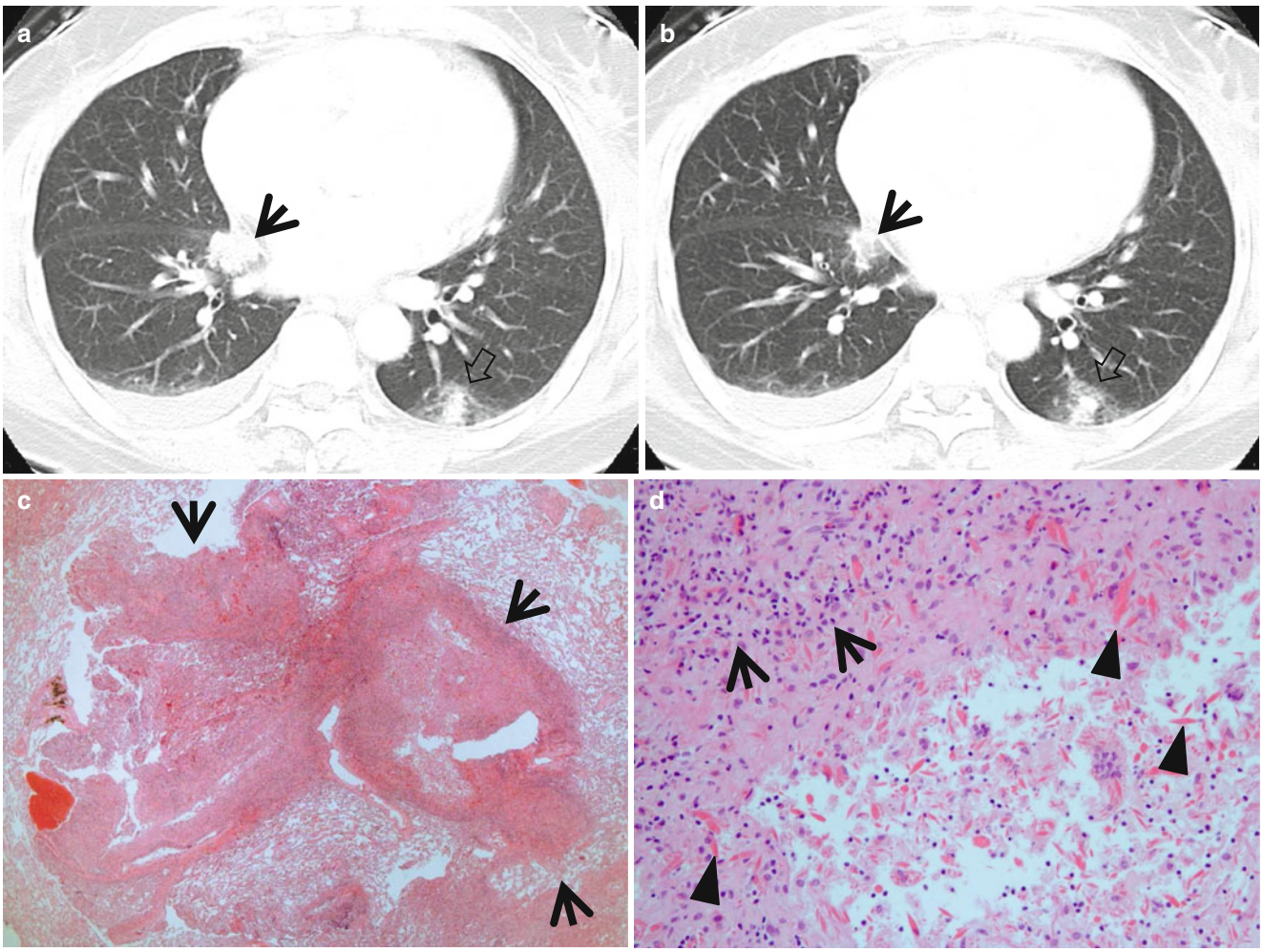

Fig. 1.16 Loeffler's (pulmonary infiltration with eosinophilia, PIE) syndrome in a 50-year-old woman. (**a**, **b**) Lung window of consecutive CT scans (5.0-mm section thickness) obtained at levels of the inferior pulmonary veins shows a nodule (*arrows* in **a** and **b**) in medial basal segment of the right lower lobe and a nodule and halo sign (*open arrows* in **a** and **b**) in superior segment of the left lower lobe. (**c**) Low-magnification (×40) photomicrograph (H & E stain) demonstrates an inflammatory nodule mainly composed of eosinophilic abscesses (*arrows*). (**d**) High-magnification (×200) photomicrograph discloses eosinophilic abscess containing granulomas (*arrows*) due to foreign-body reaction. Also note Charcot–Leyden crystals (*arrowheads*)

Symptoms and Signs

Patients are usually asymptomatic. Respiratory symptoms are minimal or absent. Malaise, fever, and cough may be present. A careful search for parasitic infection or drug reaction should be pursued.

CT Findings

TSCT findings of Loeffler's syndrome consist of GGO or airspace consolidation, usually transient and migratory, involving mainly the peripheral regions of the middle and upper lung zones, as well as single or multiple airspace nodules with surrounding GGO [35, 36] (Fig. 1.16).

CT–Pathology Comparisons

TSCT findings showing GGO or airspace consolidation involving the peripheral lung regions are histopathologically related to edema and accumulation of eosinophils in alveolar septa and interstitium [37]. A halo of GGO results histopathologically from pulmonary infiltrations of eosinophils and other inflammatory cells [52].

Patient Prognosis

By definition, this infiltration resolves spontaneously within 4 weeks. Complete resolution is the rule.

References

1. Jeong YJ, Yi CA, Lee KS. Solitary pulmonary nodules: detection, characterization, and guidance for further diagnostic workup and treatment. AJR Am J Roentgenol. 2007;188:57–68.
2. Hansell DM, Bankier AA, MacMahon H, McLoud TC, Muller NL, Remy J. Fleischner Society: glossary of terms for thoracic imaging. Radiology. 2008;246:697–722.
3. Gurney JW. Determining the likelihood of malignancy in solitary pulmonary nodules with Bayesian analysis. Part I. Theory. Radiology. 1993;186:405–13.
4. Yankelevitz DF, Reeves AP, Kostis WJ, Zhao B, Henschke CI. Small pulmonary nodules: volumetrically determined growth rates based on CT evaluation. Radiology. 2000;217:251–6.
5. Revel MP, Lefort C, Bissery A, et al. Pulmonary nodules: preliminary experience with three-dimensional evaluation. Radiology. 2004;231:459–66.
6. Marchiano A, Calabro E, Civelli E, et al. Pulmonary nodules: volume repeatability at multidetector CT lung cancer screening. Radiology. 2009;251:919–25.
7. Jeong YJ, Lee KS, Jeong SY, et al. Solitary pulmonary nodule: characterization with combined wash-in and washout features at dynamic multi-detector row CT. Radiology. 2005;237:675–83.
8. Siegelman SS, Khouri NF, Scott Jr WW, et al. Pulmonary hamartoma: CT findings. Radiology. 1986;160:313–7.
9. Lee KS, Yi CA, Jeong SY, et al. Solid or partly solid solitary pulmonary nodules: their characterization using contrast wash-in and morphologic features at helical CT. Chest. 2007;131:1516–25.
10. Jeong YJ, Lee KS. Pulmonary tuberculosis: up-to-date imaging and management. AJR Am J Roentgenol. 2008;191:834–44.
11. Travis WD, Brambilla E, Noguchi M, et al. International Association for the Study of Lung Cancer/American Thoracic Society/European Respiratory Society International Multidisciplinary Classification of Lung Adenocarcinoma. J Thorac Oncol. 2011;6:244–85.
12. Zwirewich CV, Vedal S, Miller RR, Muller NL. Solitary pulmonary nodule: high-resolution CT and radiologic-pathologic correlation. Radiology. 1991;179:469–76.
13. Yi CA, Lee KS, Kim EA, et al. Solitary pulmonary nodules: dynamic enhanced multi-detector row CT study and comparison with vascular endothelial growth factor and microvessel density. Radiology. 2004;233:191–9.
14. Godoy MC, Naidich DP. Overview and strategic management of subsolid pulmonary nodules. J Thorac Imaging. 2012;27:240–8.
15. Travis WD, Rush W, Flieder DB, et al. Survival analysis of 200 pulmonary neuroendocrine tumors with clarification of criteria for atypical carcinoid and its separation from typical carcinoid. Am J Surg Pathol. 1998;22:934–44.
16. Meisinger QC, Klein JS, Butnor KJ, Gentchos G, Leavitt BJ. CT features of peripheral pulmonary carcinoid tumors. AJR Am J Roentgenol. 2011;197:1073–80.
17. Chong S, Lee KS, Chung MJ, Han J, Kwon OJ, Kim TS. Neuroendocrine tumors of the lung: clinical, pathologic, and imaging findings. Radiographics. 2006;26:41–57; discussion 57–8.
18. Forster BB, Muller NL, Miller RR, Nelems B, Evans KG. Neuroendocrine carcinomas of the lung: clinical, radiologic, and pathologic correlation. Radiology. 1989;170:441–5.
19. Detterbeck FC. Management of carcinoid tumors. Ann Thorac Surg. 2010;89:998–1005.
20. Bae YA, Lee KS, Han J, et al. Marginal zone B-cell lymphoma of bronchus-associated lymphoid tissue: imaging findings in 21 patients. Chest. 2008;133:433–40.
21. Lee DK, Im JG, Lee KS, et al. B-cell lymphoma of bronchus-associated lymphoid tissue (BALT): CT features in 10 patients. J Comput Assist Tomogr. 2000;24:30–4.
22. Wislez M, Cadranel J, Antoine M, et al. Lymphoma of pulmonary mucosa-associated lymphoid tissue: CT scan findings and pathological correlations. Eur Respir J. 1999;14:423–9.
23. Borie R, Wislez M, Thabut G, et al. Clinical characteristics and prognostic factors of pulmonary MALT lymphoma. Eur Respir J. 2009;34:1408–16.
24. Lee JY, Lee KS, Jung KJ, et al. Pulmonary tuberculosis: CT and pathologic correlation. J Comput Assist Tomogr. 2000;24:691–8.
25. Lee KS, Im JG. CT in adults with tuberculosis of the chest: characteristic findings and role in management. AJR Am J Roentgenol. 1995;164:1361–7.
26. Sochocky S. Tuberculoma of the lung. Am Rev Tuberc. 1958;78:403–10.
27. Murayama S, Murakami J, Hashimoto S, Torii Y, Masuda K. Noncalcified pulmonary tuberculomas: CT enhancement patterns with histological correlation. J Thorac Imaging. 1995;10:91–5.
28. Lee HS, Oh JY, Lee JH, et al. Response of pulmonary tuberculomas to anti-tuberculous treatment. Eur Respir J. 2004;23:452–5.
29. Rogalla P, Lemke I, Kazmierczak B, Bullerdiek J. An identical HMGIC-LPP fusion transcript is consistently expressed in pulmonary chondroid hamartomas with t(3;12)(q27-28;q14-15). Genes Chromosomes Cancer. 2000;29:363–6.
30. Thomas JW, Staerkel GA, Whitman GJ. Pulmonary hamartoma. AJR Am J Roentgenol. 1999;172:1643.
31. Park KY, Kim SJ, Noh TW, et al. Diagnostic efficacy and characteristic feature of MRI in pulmonary hamartoma: comparison with CT, specimen MRI, and pathology. J Comput Assist Tomogr. 2008;32:919–25.
32. Potente G, Macori F, Caimi M, Mingazzini P, Volpino P. Noncalcified pulmonary hamartomas: computed tomography enhancement patterns with histologic correlation. J Thorac Imaging. 1999;14:101–4.
33. Kim GY, Kim J, Choi YS, Kim HJ, Ahn G, Han J. Sixteen cases of sclerosing hemangioma of the lung including unusual presentations. J Korean Med Sci. 2004;19:352–8.
34. Im JG, Kim WH, Han MC, et al. Sclerosing hemangiomas of the lung and interlobar fissures: CT findings. J Comput Assist Tomogr. 1994;18:34–8.
35. Chung MJ, Lee KS, Han J, Sung YM, Chong S, Kwon OJ. Pulmonary sclerosing hemangioma presenting as solitary pulmonary nodule: dynamic CT findings and histopathologic comparisons. AJR Am J Roentgenol. 2006;187:430–7.
36. Kitagawa H, Goto A, Minami M, Nakajima J, Niki T, Fukayama M. Sclerosing hemangioma of the lung with cystic appearance. Jpn J Clin Oncol. 2003;33:360–3.
37. Lee ST, Lee YC, Hsu CY, Lin CC. Bilateral multiple sclerosing hemangiomas of the lung. Chest. 1992;101:572–3.
38. Nam JE, Ryu YH, Cho SH, et al. Air-trapping zone surrounding sclerosing hemangioma of the lung. J Comput Assist Tomogr. 2002;26:358–61.
39. Sakamoto K, Okita M, Kumagiri H, Kawamura S, Takeuchi K, Mikami R. Sclerosing hemangioma isolated to the mediastinum. Ann Thorac Surg. 2003;75:1021–3.
40. Shimosato Y. Lung tumors of uncertain histogenesis. Semin Diagn Pathol. 1995;12:185–92.
41. Kim TS, Han J, Kim GY, Lee KS, Kim H, Kim J. Pulmonary inflammatory pseudotumor (inflammatory myofibroblastic tumor): CT features with pathologic correlation. J Comput Assist Tomogr. 2005;29:633–9.
42. Agrons GA, Rosado-de-Christenson ML, Kirejczyk WM, Conran RM, Stocker JT. Pulmonary inflammatory pseudotumor: radiologic features. Radiology. 1998;206:511–8.
43. Eyden B. Electron microscopy in the study of myofibroblastic lesions. Semin Diagn Pathol. 2003;20:13–24.

44. Travis WD, Hoffman GS, Leavitt RY, Pass HI, Fauci AS. Surgical pathology of the lung in Wegener's granulomatosis. Review of 87 open lung biopsies from 67 patients. Am J Surg Pathol. 1991;15:315–33.
45. Lee KS, Kim TS, Fujimoto K, et al. Thoracic manifestation of Wegener's granulomatosis: CT findings in 30 patients. Eur Radiol. 2003;13:43–51.
46. Cassan SM, Coles DT, Harrison Jr EG. The concept of limited forms of Wegener's granulomatosis. Am J Med. 1970;49:366–79.
47. Lamprecht P, Gross WL. Wegener's granulomatosis. Herz. 2004;29:47–56.
48. Kim HY, Shim YM, Lee KS, Han J, Yi CA, Kim YK. Persistent pulmonary nodular ground-glass opacity at thin-section CT: histopathologic comparisons. Radiology. 2007;245:267–75.
49. Lee HY, Lee KS. Ground-glass opacity nodules: histopathology, imaging evaluation, and clinical implications. J Thorac Imaging. 2011;26:106–18.
50. Henschke CI, Yankelevitz DF, Mirtcheva R, et al. CT screening for lung cancer: frequency and significance of part-solid and nonsolid nodules. AJR Am J Roentgenol. 2002;178:1053–7.
51. Park CM, Goo JM, Kim TJ, et al. Pulmonary nodular ground-glass opacities in patients with extrapulmonary cancers: what is their clinical significance and how can we determine whether they are malignant or benign lesions? Chest. 2008;133:1402–9.
52. Kim Y, Lee KS, Jung KJ, Han J, Kim JS, Suh JS. Halo sign on high resolution CT: findings in spectrum of pulmonary diseases with pathologic correlation. J Comput Assist Tomogr. 1999; 23:622–6.
53. Lim H, Ahn S, Lee KS, et al. Persistent pure ground-glass opacity lung nodules >10 mm in diameter at CT: histopathologic comparisons and prognostic implications. Chest 2013;144:1291–9.
54. Lee HJ, Goo JM, Lee CH, et al. Predictive CT findings of malignancy in ground-glass nodules on thin-section chest CT: the effects on radiologist performance. Eur Radiol. 2009;19:552–60.
55. Kim TJ, Goo JM, Lee KW, Park CM, Lee HJ. Clinical, pathological and thin-section CT features of persistent multiple ground-glass opacity nodules: comparison with solitary ground-glass opacity nodule. Lung Cancer. 2009;64:171–8.
56. Ullmann R, Bongiovanni M, Halbwedl I, et al. Is high-grade adenomatous hyperplasia an early bronchioloalveolar adenocarcinoma? J Pathol. 2003;201:371–6.
57. Lee HY, Lee KS, Han J, et al. Mucinous versus nonmucinous solitary pulmonary nodular bronchioloalveolar carcinoma: CT and FDG PET findings and pathologic comparisons. Lung Cancer. 2009;65:170–5.
58. Ikeda K, Awai K, Mori T, Kawanaka K, Yamashita Y, Nomori H. Differential diagnosis of ground-glass opacity nodules: CT number analysis by three-dimensional computerized quantification. Chest. 2007;132:984–90.
59. Yoshida J, Nagai K, Yokose T, et al. Limited resection trial for pulmonary ground-glass opacity nodules: fifty-case experience. J Thorac Cardiovasc Surg. 2005;129:991–6.
60. Koike T, Togashi K, Shirato T, et al. Limited resection for noninvasive bronchioloalveolar carcinoma diagnosed by intraoperative pathologic examination. Ann Thorac Surg. 2009;88:1106–11.
61. Travis WD, Garg K, Franklin WA, et al. Evolving concepts in the pathology and computed tomography imaging of lung adenocarcinoma and bronchioloalveolar carcinoma. J Clin Oncol. 2005;23:3279–87.
62. Austin JH, Garg K, Aberle D, et al. Radiologic implications of the 2011 classification of adenocarcinoma of the lung. Radiology. 2013;266:62–71.
63. Suzuki K, Kusumoto M, Watanabe S, Tsuchiya R, Asamura H. Radiologic classification of small adenocarcinoma of the lung: radiologic-pathologic correlation and its prognostic impact. Ann Thorac Surg. 2006;81:413–9.
64. Johkoh T, Muller NL, Akira M, et al. Eosinophilic lung diseases: diagnostic accuracy of thin-section CT in 111 patients. Radiology. 2000;216:773–80.
65. Noguchi M, Morikawa A, Kawasaki M, et al. Small adenocarcinoma of the lung. Histologic characteristics and prognosis. Cancer. 1995;75:2844–52.
66. Borczuk AC, Qian F, Kazeros A, et al. Invasive size is an independent predictor of survival in pulmonary adenocarcinoma. Am J Surg Pathol. 2009;33:462–9.
67. Yim J, Zhu LC, Chiriboga L, Watson HN, Goldberg JD, Moreira AL. Histologic features are important prognostic indicators in early stages lung adenocarcinomas. Mod Pathol. 2007;20:233–41.
68. Oka S, Hanagiri T, Uramoto H, et al. Surgical resection for patients with mucinous bronchioloalveolar carcinoma. Asian J Surg. 2010;33:89–93.
69. Bhatt NY, Allen JN. Update on eosinophilic lung diseases. Semin Respir Crit Care Med. 2012;33:555–71.
70. Lee HY, Jeong JY, Lee KS, et al. Solitary pulmonary nodular lung adenocarcinoma: correlation of histopathologic scoring and patient survival with imaging biomarkers. Radiology. 2012;264:884–93.